

# Monitoring deforestation in Iran, Jangal-Abr Forest using multi-temporal satellite images and spectral mixture analysis method

Neamat Karimi<sup>1</sup> · Saeed Golian<sup>2</sup> · Danesh Karimi<sup>3</sup>

Received: 12 January 2015 / Accepted: 7 October 2015 / Published online: 14 March 2016  
© Saudi Society for Geosciences 2016

**Abstract** Satellite remote sensing assessment provides a systematic and object means to quantify the rate and form of forest changes. The main objective of this study was to quantify the forest change and forest degradation in one of the oldest forests of Iran named Jangal-Abr Forest at the north of Shahrood city. Based on Landsat-TM and OLI images acquired from 1987 to 2013, four vegetation and soil fraction images were produced and compared to map the land-cover changes occurred over 26 years. Spectral mixture analysis (SMA) method was applied to estimate fraction images of the selected components over the study area. This technique examines the direction of physical changes between multi-temporal images. Then, change vector analysis (CVA) approach was used for detecting forest changes. Results revealed that during the last 26 years, 147.5 km<sup>2</sup> of forests were degraded mostly with medium severity. Part of the deforestation related to the northern and eastern regions of the study area in the vicinity of residential areas in contrast, forest regrowth area during the study period was estimated to be 62 km<sup>2</sup> typically classified with low and medium severity in the eastern parts of the study area. CVA demonstrates that deforestation in

the Jangal-Abr area has significantly accelerated from 4.6 km<sup>2</sup>/year in period 1987–2000 to about 9.6 km<sup>2</sup>/year in period 2010–2013. The rate of regrowth has been decreased gradually from 3.3 km<sup>2</sup>/year in period 1 (1987–2000) to about 0.76 km<sup>2</sup>/year in period 3 (1987–2000). By comparison the results of SMA method with Normalized Difference Vegetation Index (NDVI) changes method, it was found that except for some negligible differences, the results of both methods was very closed in terms of both spatially and the area of degradation and regrowth regions.

**Keywords** Deforestation · Remote sensing · Landsat · Spectral mixture analysis · Jangal-Abr

## Introduction

Deforestation is defined as the conversion from forest (closed, open, or fragmented forests; plantations; and forest regrowth) to non-forest lands (mosaics, natural non-forest such as shrubs or savannas, agriculture, and non-vegetated) (Achar et al. 2002). Forests still cover about 30 % of the world's land area, but swaths the size of Panama is lost each year (75,000 km<sup>2</sup>). The United Nations Food and Agricultural Organization estimated that over one million km<sup>2</sup> of the Earth's tropical rainforests and moist deciduous forests were destroyed during 1981–90, representing an annual deforestation rate of 0.75 % of such forests throughout the decade (FAO 1990). Road building, transforming forests to farming lands, ranching, logging, and fire are the most effective activities, which have devastating influence on forests worldwide. Impacts and consequences of deforestation also extend far beyond boundaries of the land directly involved with this phenomenon (Vitousek 1994).

The effects of deforestation include increasing the concentration of greenhouse gases (e.g., carbon dioxide (CO<sub>2</sub>)), and

---

✉ Neamat Karimi  
nehmatkarimi@gmail.com

Saeed Golian  
saeed\_golian@yahoo.com

Danesh Karimi  
daneshkarimi67@gmail.com

<sup>1</sup> Department of Water Resources Research, Water Research Institute, Tehran, Iran

<sup>2</sup> Civil Engineering Department, Shahrood University of Technology, Shahrood, Iran

<sup>3</sup> Department of Remote Sensing, Satellite Driven Knowledge (SDK) Institute, Tehran, Iran

consequently, the global warming and climate change increase in the rate of soil erosion and extinction of species (Avtar and Sawada 2013). In addition, the changes in forest cover could affect natural resource management, water resources, and agricultural production (Gebrehiwot et al. 2014). Deforestation not only reduces biomass stock and ecological integrity but also exacerbates flood damage (Kang and Choi 2014). The quantification and monitoring over time of this phenomenon, both inside and areas surrounding the target regions, are critical for any conservation efforts (Mas 2005; Phua et al. 2008).

Methods for estimating the rate and extent of deforestation differ widely. Satellite technology is required for the determination of deforestation due to the inaccessibility of many areas and the impracticability of aircraft-based survey methods (Tucker and Townshend 2000). From the other point of view, the accuracy of the deforestation estimates for many countries has improved greatly during the last decade, especially with increased use of satellite data and advancements in analysis techniques (Downton 1995). In general, remote sensing methods are more appropriate when degradation leads to detectable gaps in the forest canopy such as, typically, the case for selective logging or fire (Wertz-Kanounnikoff 2008). Hence, satellite remote sensing assessment provides a time and cost efficient systematic method to quantify and assess the rate and form of deforestation (Dawelbait and Morari 2012; Etteieb et al. 2013; Munyati and Kabanda 2009; Rosenberg 1992).

There are different methods for monitoring forest changes with different degree of complexity and range from simple visual interpretation of satellite imagery to highly sophisticated automated algorithms (Achard et al. 2008). Visual interpretation is labor-intensive and requires image interpreters with expert knowledge of local land-use patterns that becomes difficult when large areas require assessment and human resources are limited (Wertz-Kanounnikoff 2008). Therefore, more complex approaches than visual interpretation are usually utilized for deforestation assessment (Lunetta 1999).

In general, two main approaches have been used frequently for deforestation monitoring, i.e., vegetation indices and image classification. Vegetation indices (e.g., NDVI,<sup>1</sup> LAI<sup>2</sup>) have been used frequently to analyze forest and rangeland condition with satellite images (Dawelbait and Morari 2012; Hashemi and Fallah Chai 2013; Hashemi et al. 2013; Tucker 1979). These indices are generally based on ratios of the reflectance in the red and near-infrared spectral bands, chosen to maximize the reflectance differences between vegetation and other features (Hashemi et al. 2013). One of the most prevalent indices which have been commonly used to map temporal and spatial change of vegetation covers is the Normalized Difference Vegetation Index (NDVI) (Tucker 1979). This

index and also other similar indices are sensitive to changes in greenness and fraction of photosynthetically active radiation absorbed (Hashemi and Fallah Chai 2013; Kelarestaghi and Jafarian Jeloudar 2011). However, they are not differentially sensitive to change in vegetation cover versus vegetation conditions. On the other hands, when NDVI change occurs, it cannot be readily determined whether or not it was caused by condition of vegetation cover or altered vegetation cover (Asner et al. 2004). Image classification methods are usually based on statistical analyses including minimum distance, maximum likelihood, etc. (Kelarestaghi and Jafarian Jeloudar 2011); however, for deforestation monitoring and to obtain precise measurement, the spatial resolution of image must be smaller than the variability scale of at least one of the principle landscape features.

In addition to the aforementioned drawbacks of vegetation indices and classification techniques, mixed pixels are another factor which affects the accuracy of deforestation monitoring. Mixed pixels (pixels with more than one feature in each) are common in medium spatial resolution remotely sensed data, and such pixels have been recognized as a problem for remote sensing applications (Cracknell 1998; Fisher 1997). To deal with mixed pixels, spectral mixture analysis (SMA) approach has long been used as an effective method for improving analyses accuracy (Adams et al. 1995). SMA is a method for transforming a mixed pixel in a satellite image into a proportion of spectrally defined land-cover types (Elmore et al. 2000; Shimabukuro and Smith 1991). SMA depends on the spectral response of land-cover components. The spectral response in remote sensing from open canopies is a function of the number and type of reflecting components, their optical properties, and relative proportions (Adams et al. 1995).

(Anderson et al. 2005) developed a method for using MODIS data through the mixing algorithm as a basis for deforestation alert system. In their mixing model, three endmembers, namely vegetation, soil, and shade, were used. They used Landsat-ETM+ data for validation. Results showed the robustness of the technique applied to the MODIS data for deforestation detection. Dawelbait and Morari (2012) applied SMA method along with change vector analysis (CVA) to Landsat images to monitor land-cover degradation in Savana region in Sudan. The results showed the consistency of their method in obtaining information on vegetation cover, soil surface type, and identifying risk areas.

In general, not a lot of studies are found regarding deforestation in Iran. Some studies examined the impact of some social factors and land-use changes on deforestation in the North of Iran (Esmaeili and Nasrnia 2014; Kavian et al. 2014).

In this paper, we examine the application of SMA method to assess forest change in Iran, over the Jangal-Abr Forest using Landsat images during 1987–2013. This paper is going to address the question raised by many NGOs which believe that during last three decades, deforestation has largely

<sup>1</sup> Normalized Difference Vegetation Index

<sup>2</sup> Leaf-Area Index

occurred in the region. In addition, the paper aims to determine the location of forest changes. The structure of the paper is as follows: in “Case study region” section, a concise description about the case study area and data used is presented. Then in “Materials and methods” section, the methodology including method of end member selection, linear spectral mixture analysis (LSMA), and change vector analysis are described. Finally, the results and discussions of applying SMA method to the study area are assessed and evaluated with NDVI differences in “Results and discussions” section. At the end of this section, conclusions are presented.

### Case study region

Generally, Iran has an arid and semi-arid climate in which most of the relatively scant annual precipitation falls from October to April. In most of the country, yearly precipitation averages 250 mm or less. Iran’s precipitation decreases going from north to south and from west to east, with the highest precipitation prevailing in the northern regions of the country and the lowest in the southern locations. Therefore, according to this general rule, most forest covers of Iran are concentrated in the north and northwestern part of Iran.

Despite meager rainfall in Iran, 7 % of the country is forested (about 115,000 km<sup>2</sup>) (FAO 2003). The most extensive growths are found on the mountain slopes rising from the Caspian Sea, with stands of oak, ash, elm, cypress, and other valuable trees. Forested ecosystems in Iran are undergoing accelerated degradation due to several natural and anthropogenic disturbances. The annual rate of deforestation in Iran is 2.3 % in the northern part of the country and 1.1 % in other regions (Abbasi and Mohammadzadeh 2001; Esmaeili and Nasmia 2014). The main causes of these changes in Iran are as follows: conversion of forests to agricultural land, the summer wildfires, overgrazing, clear cutting (for residential development), and wood fuel use (Amirnejad et al. 2006). Using environmental Kuznets curve (EKC) model, Esmaeili and Nasmia (2014) concluded that improvement of secure property rights and environmental policies could improve and reduce the deforestation rate in Iran.

Jangal-Abr (Cloud Forest) is one of the oldest forests in Iran located between Semnan and Golestan provinces (Fig. 1). It is the continuum of northern forests in the south of Alborz mountain range. The area in most seasons is overcast and foggy. Natural vegetation consists of oak tree, maple, alder, pasture plant species, thyme, and clover. Virgin Jangal-Abr Forest has remained of the third geological period and the age of some trees in this forest exceed 4000 years. It has approximately 25,000 ha area, which is located at the longitude of 55.08 and latitude of 36.70. Jangal-Abr has an annual precipitation of 300 to 400 mm (which is correlated with elevation) and maximum and minimum temperature of 20 and

0.6 (°C), respectively. Generally, this region has moderate temperature, varying seasonally between hot and cool seasons. Due to a diverse situation of climate and topographic factors, a complex mosaic of diverse vegetation exists.

It is believed (but has not proved yet) that because of some human activities, e.g., road construction, recently conducted in this area, the deforestation has been accelerated in the past few years. The objective of this study is to quantify the amount of deforestation and forest regrowth in this region using remote sensing techniques.

## Materials and methods

### Satellite data and preprocessing

With regard to frequent rainy and cloudy weather conditions in our case study area, only a few cloud-free remotely sensed imagery exist (i.e., lower than 10 % cloud cover). To account for deforestation analysis, four Landsat images (acquired on May 22, 1987, May 25, 2000, June 6, 2010, and June 14, 2013) were analyzed (Row=35, Path=162) to generate historical and recent vegetation maps of the study area, showing deforestation over a 26-year period. These near-anniversary image dates were used to ensure a minimum number of exogenous effects (e.g., soil moisture content and minimal sun angle effects). The time interval for period 1987–2000 was relatively long because available satellite images between those dates were typically obscured by cloud cover. Also, Landsat images were selected because their frequency of monitoring is high and their coverage is appropriate for monitoring the environmental conditions in a large geographic zone. In present study, all visible, infrared and near-infrared bands in Landsat images were used for spectral analysis. These wavelengths include bands 1 to 7 in Landsat-5 TM images (with the exception of thermal bands (band 6)) and bands 2 to 7 in Landsat-8 OLI image. The wavelengths of above bands in Landsat-5 and 8 are quite consistent with each other.

One of the most important factors considered in selecting the images is the absence of any seasonal vegetation cover change in each image. It means, due to the seasonal variations in vegetation covers, the images’ acquisition time must be similar to each other. So, here in this study, all images were acquired from the end of May to the first half of June with maximum 22 days interval (Table 1).

The first three Landsat images are acquired from Landsat-5-TM, which has 7 bands, 6 in the optical with 30 m spatial resolution. Due to the existence of VIS (Visible) and NIR (Near Infrared) bands, Landsat images are capable of clearly differentiating vegetation cover regions from other surfaces. Landsat scenes were acquired under excellent conditions (includes cloud-free and no seasonal snow cover around the forested region).

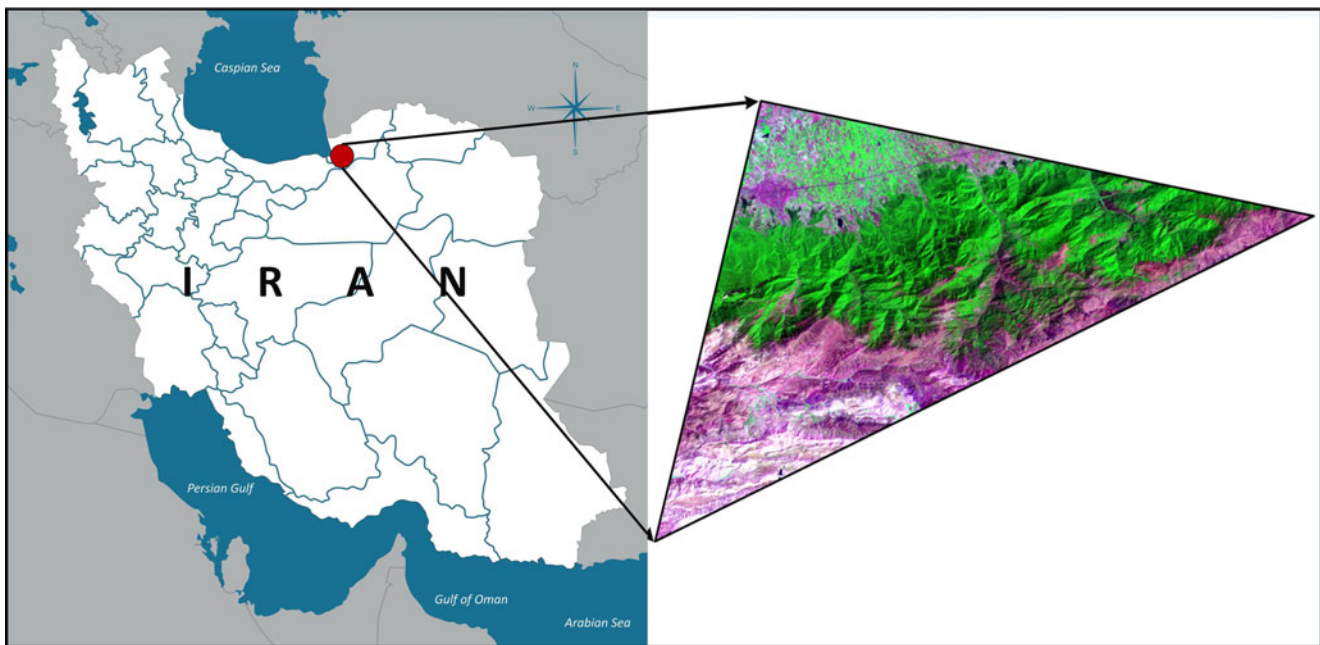


**Fig. 1** Location of the study area and its topographical status

Also, the last image acquired from Landsat-8. Landsat-8 is an American Earth observation satellite launched on February 11, 2013. It is the eighth satellite in the Landsat program; the seventh to reach orbit successfully. Originally called the Landsat Data Continuity Mission (LDCM), it is a collaboration between NASA and the United States Geological Survey (USGS). Providing moderate-resolution imagery, from 15 to 100 m, of Earth's land surface and polar regions, Landsat-8 will operate in the visible (4 bands), near-infrared (1 band), short wave infrared (3 bands), thermal infrared (2 bands) spectrums, and panchromatic image (1 band) all with 12 bit radiometric resolution.

After acquiring appropriate satellite images, two separate pre-processing have been done in the present paper. These pre-processing includes the co-registration of successive images at sub-pixel level and atmospheric correction. For accurate detection of land-cover changes, it is necessary to ensure that the images from different times are co-registered precisely with a root-mean-square error (RMSE) of no more than one pixel (Munyati 2000). In this regard, three old images (TM-1987, 2000, and 2010) were registered to the Landsat-8-2013 by collecting 28 ground control points (GCPs) for each image pair. This co-registration is partially easy because of the distinct

phenomena and features over our study area. The mean RMSE for the registration of all images to the TM-2013 is about 8 m (0.26 pixels).

To acquire any remote sensing image, the solar radiation should pass through the atmosphere before the instrument can collect it. Because of this fact, remotely sensed images include information about both the atmosphere and the earth's surface. For those interested in quantitative analysis of surface reflectance, removing the influence of the atmosphere is a critical preprocessing step (Bernstein et al. 2006). While several atmospheric correction modules exist, but due to lack of appropriate ancillary data (e.g., information on atmospheric conditions of case study region), we could not apply them in our study. Hence, only the dark object subtraction approach was used. As a result, the brightness values were corrected for path radiance and normalized for seasonal variability and other attributing factors.

### Spectral mixture analysis method

In satellite images, due to the high variability in the distribution of land-cover components, the pixels usually contain mixed spectral information. Spectral mixture analysis is based

**Table 1** Scene characteristics for Landsat data

Sensor	Acquisition date	SCENE-ID	Illumination	
			Sun elevation (°)	Sun azimuth (°)
Landsat-5-TM	1987-05-22	LT51620351987142XXX02	60.10	113.9
Landsat-5-TM	2000-05-25	LT51620352000146XXX02	62.64	116.2
Landsat-5-TM	2010-06-06	LT51620352010157KHC00	66.04	117.7
Landsat-8-LCDM	2013-06-14	LC81620352013165LGN00	68.25	119.7



on this concept that pixel spectral response is a function of the weighted average of the objects within it. It means SMA transforms the reflectance of all pixels into fractions of a few dominant endmembers. This technique assumes that the reflection of an image pixel represents the average of the spectral responses of its dominant components and for ease of application usually uses a linear relationship to represent their spectral mixture. Therefore, if the spectral responses of pure components are known, the proportions of each component can be estimated for any given pixel in an image (Shimabukuro and Smith 1991). In other words, SMA was used to generate the relatively proportions for water, vegetation, soils, and each other endmembers dominated in the study area. These proportions (which have been extracted at different times) were then used to detect deforestation.

The value of sub-pixel fraction maps provided by SMA has been demonstrated in climate change research, ecosystem monitoring and management, precision agriculture and production monitoring, natural hazard risk assessment, forest inventories and forest health assessments, desertification monitoring, water quality assessment, geological mapping, and extraterrestrial mapping surveys (Moridnejad et al. 2015; Somers et al. 2011). Present approach has been used frequently for deforestation and forest/rangeland degradation monitoring. For example, SMA method was used to assess postfire vegetation regeneration in Peloponnese (Greece) wildfires using Landsat images (Veraverbeke et al. 2012). Based on results obtained in this study, authors found both simple SMA and multiple endmember SMA have good abilities for detecting the postfire vegetation recovery in mixed vegetation–substrate environments which makes spectral mixture analysis (SMA) a very effective tool to derive fractional vegetation cover maps. Also, in another study, weighted multiple endmember spectral mixture analysis (wMESMA) method was used over a Eucalyptus globulus plantation in southern Australia for defoliation monitoring (as a key parameter of forest health and is associated with reduced productivity and tree mortality) (Somers et al. 2010). Authors found that the results of SMA can be significantly improved by the inclusion of an age correction algorithm for both the multi-spectral (Landsat images) and hyperspectral (Hyperion images) image data. In central San Luis Province (Argentina), where signs of severe landscape degradation have been observed in the last decades, two Landsat satellite images were used to evaluate the potential of SMA method in desertification and vegetation degradation monitoring (Collado et al. 2002). Results shows that information generated from SMA of Landsat images is valuable to monitor signs of desertification processes connected to land-use mismanagement in relation to rainfall patterns. In other study, the capability of fractional images (derived from SMA method) and NDVI index were tested for grassland degradation around the built-up area of the city using the combination of vegetation fraction images, sand fraction images,

and NDVI images (Guang-jun et al. 2009). This research found that fractional images of vegetation and sand have good potentiality for vegetation degradation detection over the mixed areas of regions around the city areas. In another study, the efficiency of SMA method in monitoring the land-cover changes in semi-arid environment has been evaluated (Khiry and Csaplovics 2007). Results indicate that SMA technique is powerful for characterization and mapping of land degradation by providing direct measure of different land cover. Generally, it can be emphasized that SMA provides an invaluable tool for detecting and mapping land-cover/use changes by offering more detailed information at sub-pixel level. Application of operational multi-temporal remote sensing data (such as Landsat satellite images) demonstrate that it is possible to apply SMA efficiently in efforts to optimize the detection and analysis of local and regional land-cover/land-use changes.

Generally, SMA procedure involves three steps: (a) evaluating the number of specific materials in a scene (for obtaining the endmembers); (b) selection of the physical features of each endmember; (c) determining the fraction of each endmember in all pixels. An outline of the data processing flow for deforestation detection using SMA remote sensing method is shown in Fig. 2.

*Linear spectral mixture analysis*

The basic LSMA equation is (Dawelbait and Morari 2012):

$$R_p(\lambda) = \sum_{i=1}^n f_i R_i(\lambda) + \varepsilon(\lambda) \tag{1}$$

where  $R_p(\lambda)$  is the apparent surface reflectance of a pixel in an image,  $f_i$  is the weighting coefficient ( $\sum_{i=1}^n f_i = 1$ ) interpreted as fraction of the pixel made up of the endmember  $i = 1, 2, \dots, n$ ,  $R_i(\lambda)$  is the reflectance spectrum of spectral endmember in an n-endmember model, and  $\varepsilon(\lambda)$  is the difference between the actual and modeled reflectance.  $f_i$  represents the best fit coefficient that minimizes RMS error given by the following equation:

$$RMS = \left[ \frac{\sum_{j=1}^m (\varepsilon_j)^2}{m} \right]^{0.5} \tag{2}$$

where  $\varepsilon_j$  is the error term for each of the  $m$  spectral bands considered.

One of the main features of SMA methods is their ability to compare data from different sensors. It is more likely that researches can acquire images that are not obscured by

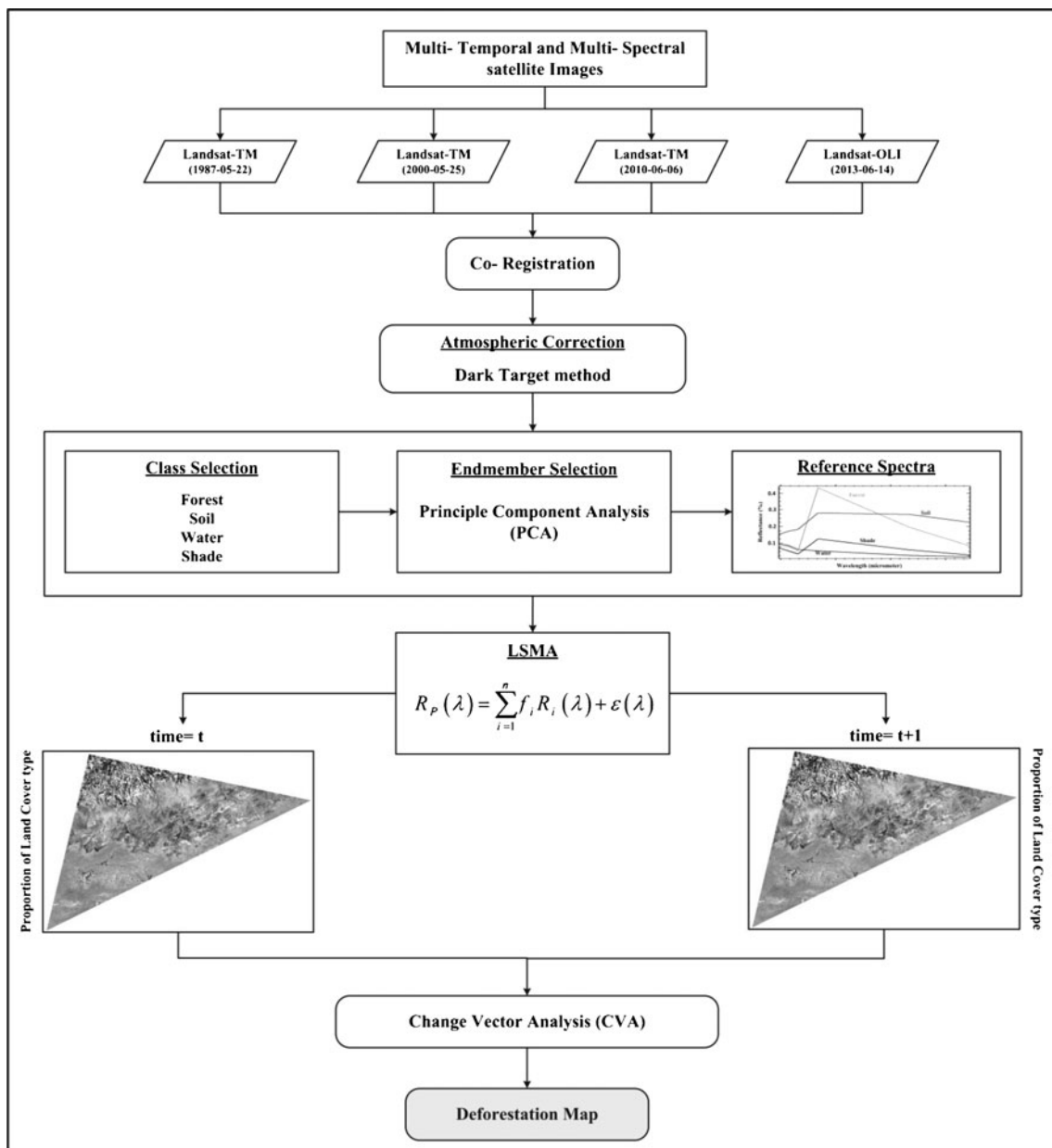


**Fig. 2** The process of deforestation map extraction using spectral mixture analysis method

cloud cover than if images came from a single source. This ability is very entrepreneur and extremely helpful in the present study. As noted previously, Jangal-Abr in most cases is cloudy. Therefore, the inevitable need for multi-sensor analytical methods necessitates further investigations into this approach and its application for monitoring Jangal-Abr deforestation.

#### Endmember selection

The following pure components (endmembers) were defined for this study: soil, vegetation cover, water bodies, and shaded areas. Present endmembers have been used frequently for

deforestation monitoring (Adams et al. 1995). Indeed, previous studies have found that the dimensionality of Landsat-TM and ETM+ satellite images suited to spectral unmixing. Selecting these endmembers can help examining four vegetation and non-vegetation change categories in present study: (A) No changes, (B) vegetation increase (natural or anthropological), (C) vegetation decrease (repeatedly summer fires, vegetation cleaning, effect of climate oscillations, and sequential droughts), (D) recharge or flooding in probable reservoirs and lakes.

Some SMA approaches use endmember spectra derived from the image (image endmember) (Wessman et al. 1997), whereas others employ endmembers collected from spectral

measurements in the field or laboratory (library endmember), which are produced from reflectance measurement in a laboratory (Smith et al. 1985). The extraction of endmembers from the images reduces the potential noise related to the atmospheric or radiometric correction of the images (Collado et al. 2002). On the other hand, library endmember method needs much effort to gather and atmospherically correct field or laboratory spectra.

In this study, principle component analysis (PCA) was applied to derive endmembers from image data (Bryant 1996; Smith et al. 1985). The first step is to calculate principal components for the Landsat images. Principal components are orthogonal and linear transformations of the original image values, in which  $N$  original, highly correlated bands (i.e., six bands in the case of Landsat images) are transformed into  $N$  new, uncorrelated bands (principal components). The first two principal components, typically explaining more than 90 % of the original variance, are plotted in a scatter plot diagram. The

corners of the polygon bounding the scatter of data points represent the location of the purest and thus endmember pixels. Some of these points can be checked randomly by field survey.

As illustrated in Fig. 3, PCA was applied to TM images by means of ENVI software to identify appropriate endmembers. As it was observable in Fig. 3, the scatter plot of the first three principle components produced a triangle in which the pure endmembers were located at the corners. Present approach has been applied frequently for identifying an appropriate endmembers in several studies (Brandt and Townsend 2006; Jacobson 2014; Small 2001, 2004). After identifying pure endmembers for all classes, spectral libraries for each classes were derived based on the wavelengths of Landsat bands (Fig. 3d). These spectra were used in LSMA model. This model measures the reflectance of a pixel in each spectra bands as a linear combination of the reflectance of its component endmembers, weighted by their respective surface

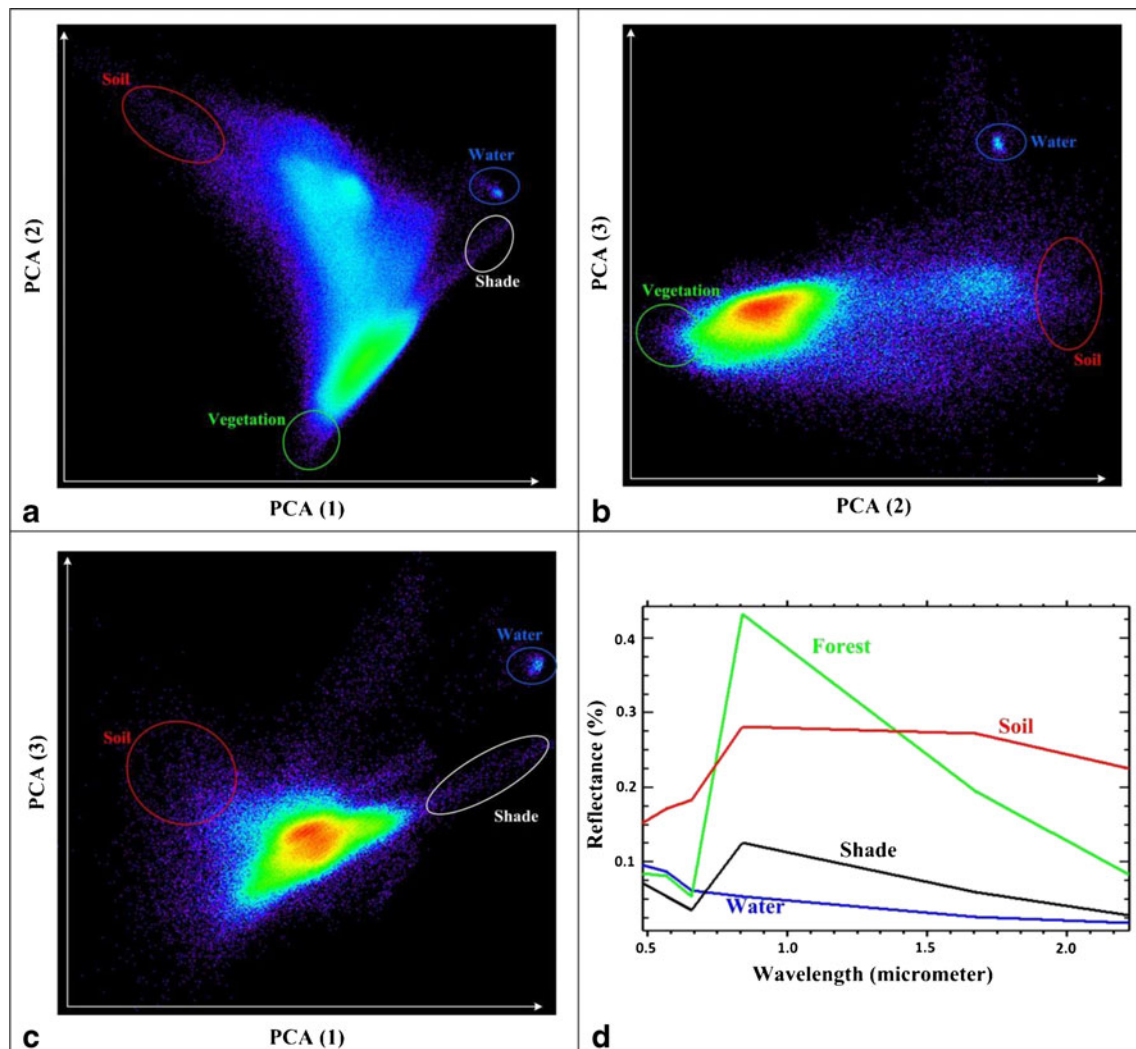


**Fig. 3** Combination of **a** first and second, **b** second and third, and **c** first and third PCA for identifying endmembers. Part **d** shows the spectra of the selected endmembers

proportion. Endmember spectra were applied to Linear SMA in order to produce the fraction images which associated the RMSE images. Figure 4 shows the fraction of forest and soil covers with associated RMSE images for TM-1987 image.

### Change vector analysis

After producing the fraction images of each selected classes, change vector analysis (CVA) approach was used for detecting and characterizing forest changes. CVA can detect the direction (the nature of the change) and magnitude (length of the change) of change from the first to second date in a spectral change vector. In the present study, the magnitude of vectors was measured among spectral changes between the endmember fraction images of dates 1987, 2000, 2010, and 2013. In this regard, fraction of vegetation was placed along the *X*-axis and the fraction of soil placed along *Y*-axis (Fig. 5). Then, the magnitude of the vector was calculated from the Euclidian Distance formula. In addition, the direction of change was measured as the angle of the change vector from pixel measurement at 1987 to the corresponding pixel measurement at 2013, for example, according to following equation:

$$\tan \alpha = (\text{soil}_{1987} - \text{soil}_{2010}) / (\text{vegetation}_{1987} - \text{vegetation}_{2010}) \quad (3)$$

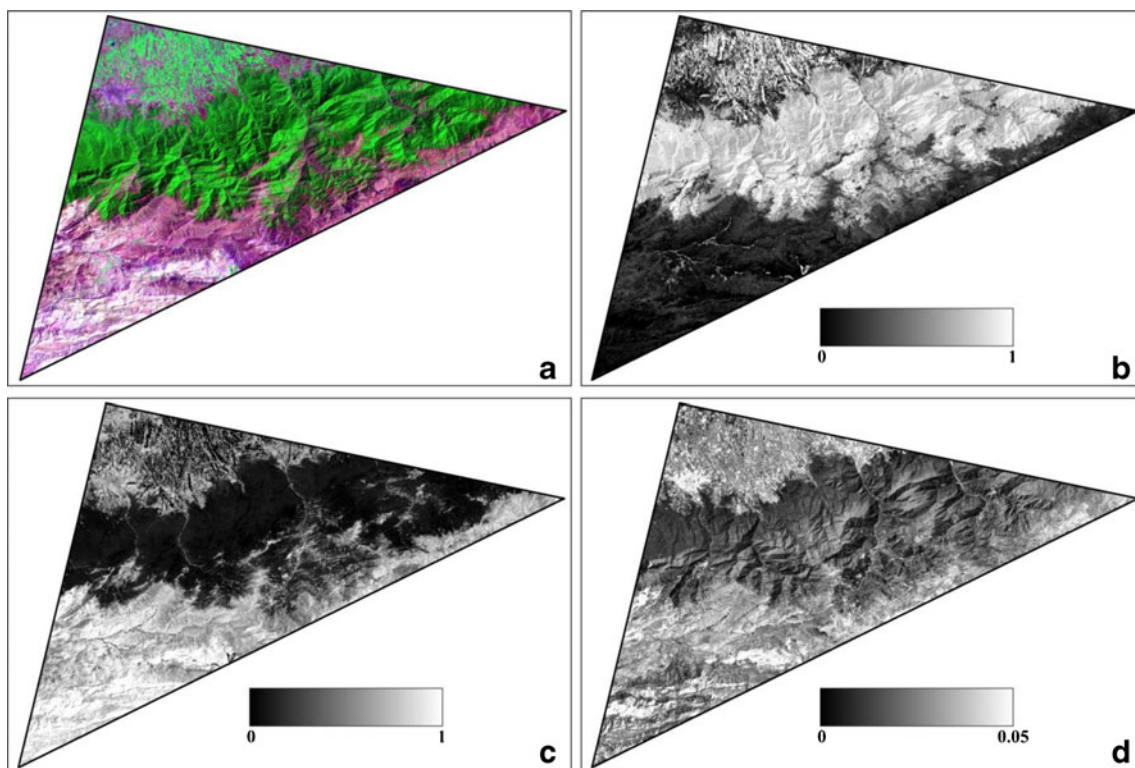
Angles measured between  $90^\circ$  and  $180^\circ$  indicate an increase in soil and a decrease in vegetation and thus a deforestation situation. Angles between  $270$  and  $360$  indicate a decrease in

soil and an increase in vegetation and therefore represent a regrowth condition (Dawelbait and Morari 2012). The process of direct measurements is described briefly in Fig. 5.

### Results and discussions

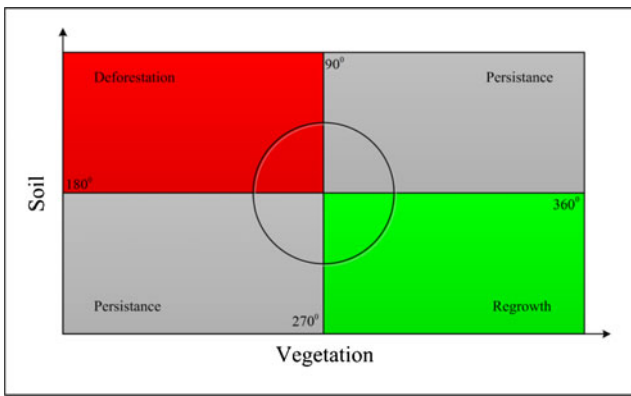
Based on SMA method described in the previous section, the fraction of forest and soil covers and associated error (RMS) images were calculated. Figure 4 represents derived values for May 1987, as an example. Using CVA method, the magnitude and direction of the change are shown by the length and angle of the vector, respectively. This method computes the magnitude of the changes per pixel by determining the Euclidean distance between the end points through *n*-dimensional space. At the end, the amount of deforestation/regrowth was categorized into low, medium, and high.

Figure 6 shows that the magnitude of deforestation and regrowth ranges from low to high (extreme), with a prevalence of severe deforestation conditions (high) mostly in the northern part of study area. Also, medium deforestation has generally occurred in the center and eastern parts of the study area. Change detection analysis also showed the existence of high regrowth conditions over the last 26 years (between 1987 and 2013) spread in the eastern parts. Generally, deforestation prevailed over regrowth (Figs. 6 and 7) affecting an area of  $147.5 \text{ km}^2$ , with a prevalence of medium ( $58.7 \text{ km}^2$ ) class of magnitude between 1987 and 2013. This is while the regrowth



**Fig. 4** Map of **a** RGB TM image and fraction of **b** forest and **c** soil covers with **d** associated RMS error (Equation 2) for May 1987





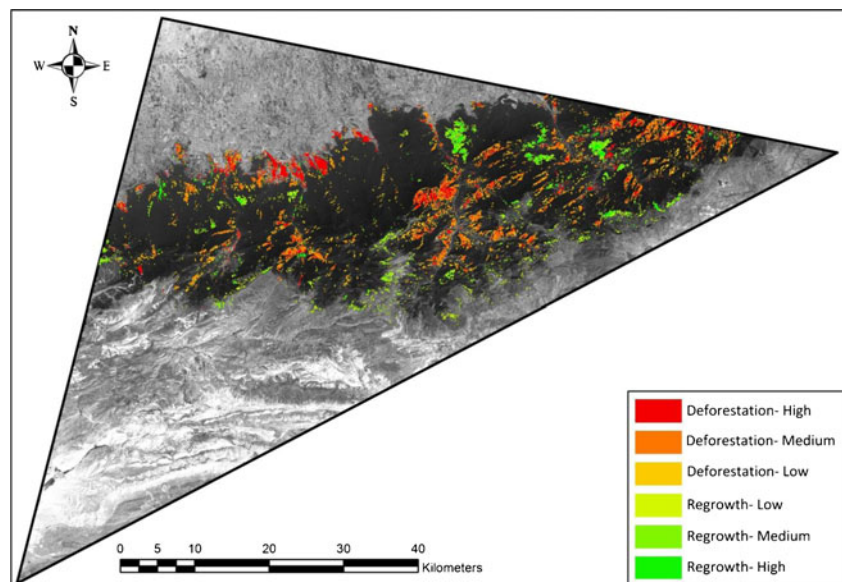
**Fig. 5** The procedure for detecting the direction of forest change (deforestation, regrowth, or persistence) (Dawelbait and Morani, 2011)

condition was estimated on an area of 62.03 km<sup>2</sup>, mainly classified as low (27.8 km<sup>2</sup>).

Deforestation during period 1 (1987–2000) was 60.3 km<sup>2</sup> while deforestation during period 2 (2000–2010) was 34 km<sup>2</sup> as indicated in Table 2. Also, during period 3 (2010–2013), desertification was about 30 km<sup>2</sup>. In the same way, regrowth during periods 1, 2, and 3 were about 43, 23, and 2.3 km<sup>2</sup>, respectively. This means that the total area of deforestation and regrowth during the time intervals of study have been decreased gradually. This is because of different time intervals between selected images. It means the first period (1987–2000) is longer than the latest periods. Thus, for better analyzing the temporal change of deforestation, deforestation should be interpreted during different periods. Table 2 contains the area of regions exposed to each class of deforestation/regrowth condition where the total rate of deforestation/regrowth included in the last row.

The rates of deforestation/regrowth for different time intervals are shown in Fig. 8. It is apparent that deforestation rate for all severity classes, i.e. high, medium, and low, has increased significantly in the last interval, i.e., from 2010 to

**Fig. 6** Deforestation and regrowth areas calculated by applying change vector analysis (during 1987–2013)



2013. In period 1, the deforestation rate is about 4.6 km<sup>2</sup>/year, while during period 2, the deforestation rate has decreased to about 3.4 km<sup>2</sup>/year. After 2010, the deforestation rate has been increased significantly to about 9.6 km<sup>2</sup>/year. Unlike deforestation, the regrowth rate does not show any fluctuations. It means the rate of regrowth has been decreased gradually from 3.3 km<sup>2</sup>/year in period 1 to about 0.76 km<sup>2</sup>/year in period 3. The rate of decline in low and medium regrowth classes are approximately equal (about 0.65 km<sup>2</sup>/year), but the rate of high regrowth is quite different from previous classes (about 0.27 km<sup>2</sup>/year). It means the rate of low and medium regrowth is about 2.5 times greater than the high regrowth class.

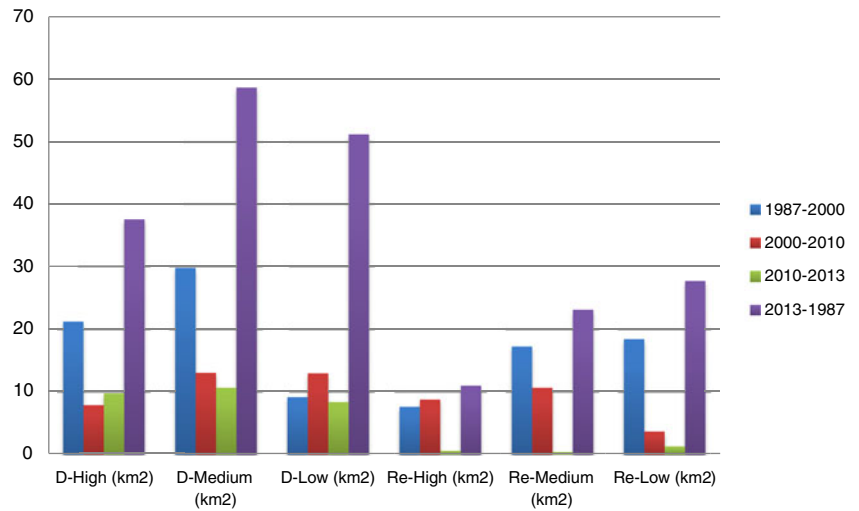
For evaluating the results of SMA method, time series of Normalized Difference Vegetation Index (NDVI) derived from Landsat satellite images were used quantitatively. Although this index has some constraints for deforestation monitoring (as mentioned previously), but this index represents the approximation relation between the spectral response and vegetation cover. Changes in NDVI index can reflect the changing processes of land productivity. Therefore, this index was used as deforestation monitoring indicator to monitor deforestation and dynamic changes.

The Normalized Difference Vegetation Index (NDVI) is one of the most well known and most frequently used index for monitoring vegetation health, stress, changes, and distinguishing between different vegetation types. The combination of its normalized difference formulation and use of the highest absorption and reflectance regions of chlorophyll make it robust over a wide range of conditions. NDVI is defined by the following equation:

$$NDVI = (NIR - Red) / (NIR + R) \tag{4}$$

The value of this index ranges from -1 to 1, while the common range for vegetation cover is 0.2 to 0.8.

**Fig. 7** Area of deforestation and regrowth classes for Jangal-Abr study area



NDVI index were calculated for all Landsat images used (1987, 2000, 2010, and 2013), and then differencing of the images were carried out to detect deforestation during each time periods. Differencing involved the subtraction of the 2013 NDVI image from the earlier NDVI images using an image calculator in the software. In other hand, after calculating NDVI for each Landsat satellite image, the raster layer, which can be used to assess deforestation over time, is created by subtracting NDVIs. Figure 9a, b illustrates longer term (1987–2013) NDVI changes and histogram data for NDVI difference of the area under study, respectively. In this figure, the positive and negative of NDVI differences are an indication of regrowth and reduction of forest cover, respectively.

As illustrated in Fig. 9a, the spatial distribution of NDVI change in the period of 1987–2013 is very similar to the SMA method. In both approaches used, no change areas are predominated. Also, a negative evolution of the NDVI index which was indicating a deforestation area was also observed in several parts of the case study region. A decrease in the NDVI dominated the northern (marked as “A”) and central parts of the study area (marked as “B”), whereas in the central

of Jangal-Abr forest, the pattern was partially patchy. Unlike deforested areas (negative value of NDVI changes), the regrowth regions do not have a specific spatial patterns and irregularly distributed in different parts of the study region. Also, these areas comprised a small percentage of the total surface area. These achievements are much closed to the results of SMA method used.

Figure 9b shows the frequency distribution of the magnitude of the NDVI changes during 1987–2013. The pattern indicates a high percentage of areas with no significant NDVI changes (between  $-0.05$  and  $+0.1$ ) in comparison with perceptible negative and positive changes. Based on obtained results, the areas of deforested regions are about  $130 \text{ km}^2$  which is about 11 % smaller than the SMA method used (about  $147.5 \text{ km}^2$  in SMA) within a period of 26 years between 1987 and 2013. Unlike deforested results, the amount of regrowth regions is overestimated. It means the areas with positive NDVI differences are about  $73 \text{ km}^2$  which is 17 % greater than the SMA method (about  $62 \text{ km}^2$  in SMA).

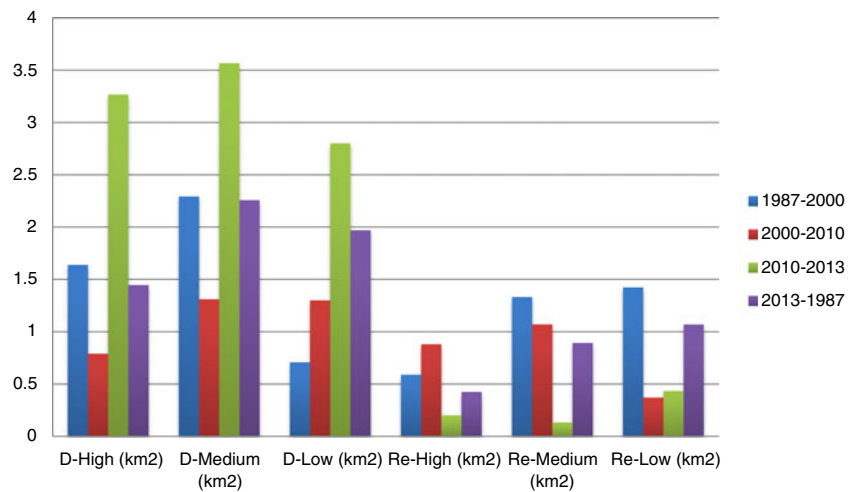
To investigate the role of urban/rural development on both deforestation and regrowth conditions, the locations of all residential areas were mapped and shown in Fig. 10. It is obvious that there is a direct relationship between deforestation and existence of residential areas. For example, as shown in Fig. 10 (marked as “A”), high concentration of residential areas has caused deforestation with high severity in urban/rural areas compared to other regions with no/very limited residential districts. Also, it can be seen that for the central part of the study area in the absence of residential areas, there is not any sign of deforestation/regrowth (marked as “B” in Fig. 10). As a result, it can be concluded that the main cause of deforestation in this region is related to anthropogenic factors (e.g., road construction, construction of residential areas, overgrazing, and supply of fuel) rather than natural ones.

For evaluating the reasons of deforestation over our case study region, climatological factors (prevalently influenced by

**Table 2** Area and rate of deforestation/regrowth conditions for different time intervals between selected images used for Jangal-Abr

Class	1987–2000	2000–2010	2010–2013	2013–1987
D-high (km <sup>2</sup> )	21.3	7.9	9.8	37.6
D-medium (km <sup>2</sup> )	29.8	13.1	10.7	58.7
D-low (km <sup>2</sup> )	9.2	13	8.4	51.2
Re-high (km <sup>2</sup> )	7.66	8.8	0.6	11.03
Re-medium (km <sup>2</sup> )	17.3	10.7	0.4	23.2
Re-low (km <sup>2</sup> )	18.5	3.7	1.3	27.8
Deforestation rate (km <sup>2</sup> /year)	4.6	3.4	9.6	5.67
Regrowth rate (km <sup>2</sup> /year)	3.3	2.3	0.76	2.38

**Fig. 8** Rate of deforestation and regrowth for each classes in Jangal-Abr study area



precipitation) should be analyzed in addition to anthropological factors. Evaluating the precipitation trends during the periods can show the relationship between climate changes and forest changes more clearly. In our study region, there are no weather stations and these relationships cannot be analyzed in more details. The precipitation data were derived from GPCP<sup>3</sup> (<http://disc.sci.gsfc.nasa.gov/giovanni>). In present project, data from over 6000 rain gauge stations, and satellite geostationary and low-orbit infrared, passive microwave, and sounding observations have been merged to estimate monthly rainfall from 1979 to the present. In Fig. 11, the monthly changes in precipitation from 1979 to 2013 are shown. As illustrated in Fig. 11, during the last 34 years, the precipitation gradually decreased. Based on this analysis, the annual precipitation of this region over the past 34 years about 37 mm has decreased (about 10 %).

In general, the deforestation areas can be classified into two categories: anthropogenic (non-renewable) and natural forest degradation (renewable). The category is related to the areas that have been deliberately destroyed in order to produce timber or changed to provide residential areas. An example of these regions is shown in Fig. 12a. This type of deforestation is almost limited in our study area (since Jangal-Abr Forest is one of the protected areas in Iran). Nevertheless, an important point that should be noted is that the deforestation of anthropogenic type is very persistence compared to natural forest degradation. In the case of fires or droughts where some parts of the forests are degraded, with a normal weather condition, the destroyed regions could be recovered and the land cover would return to its regular condition over the upcoming years. This is while in the regions anthropogenic deforestation, e.g., as the result of constructing the settlements, the chance for recovery is very low. Several parts of the study region were destroyed because of natural catastrophes, i.e., consecutive droughts and numerous forest fires. Figure 12b shows an

example of these regions which has been destroyed due to the fires. This type of damage is the most common form of forest degradation in this region. Several reports indicate that between the years 2009 and 2013, 80 cases of forest fires with different degrees of severity and extension and coverage have been occurred in the study region.

Similar to deforestation regions, regrowth areas could be classified into two different types based on the mechanism of forest regrowth. The first type of regrowth is related to regions where reforestation (regrowth) and plant seeding have been implemented by relevant organizations (e.g., forest Management Bureau) (Fig. 13a). Indeed, according to reports published by governmental organizations, various forestation projects have been implemented in the past years in this area. For example, since 1992, about 11 thousand hectares of this region is forested. In addition, more than 200 acres have been excluded from other regions and forested exclusively.

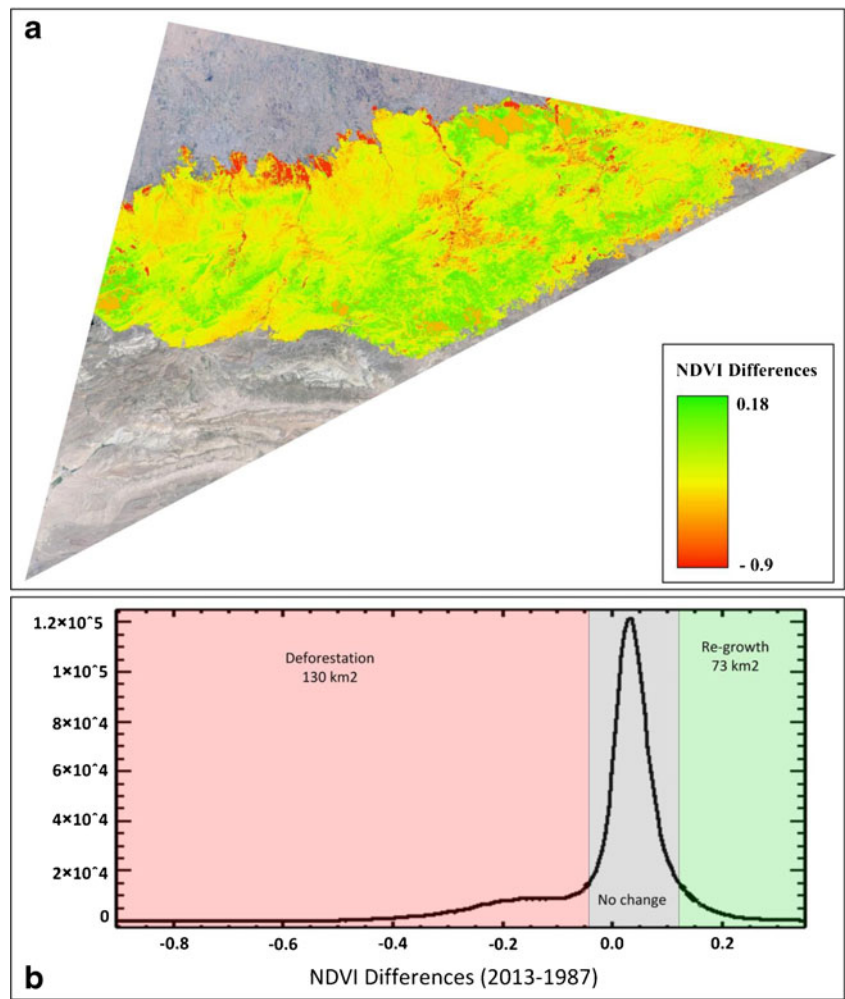
Unlike the pervious type of forestation, several regrowth can be observed due to the natural regrowth of forests after fires or droughts (Fig. 13b). It should be noted that the ability of a tree to withstand fire damage and regrowth conditions is based on several parameters, e.g., the thickness of the bark, rooting depth, needle length, bud size, and degree of scorch. As shown in Fig. 13b, several parts of the study region regrowth normally after 26 years and this kind of reforestation is more dominant in our study region.

**Conclusion**

Information generated from spectral mixture analysis (SMA) of Landsat images is valuable to monitor forest changes and detect the amount and the spatial/temporal distribution of changes. In this study, the analysis of four images acquired in 1987, 2000, 2010, and 2013 showed regions which are exposed to deforestation/regrowth conditions with different levels of severity.

<sup>3</sup> Global Precipitation and Climatology Project

**Fig. 9** **a** Spatial distribution of the magnitude of the NDVI changes between the 1987 and 2013. **b** The histogram of NDVI changes between 1987 and 2013



Results revealed that deforestation affected 147.5 km<sup>2</sup> of the forests from 1987 to 2013, mostly with medium severity.

Meanwhile, regrowth influenced approximately 62 km<sup>2</sup> mainly classified as low severity. Based on change detection

**Fig. 10** The location of residential areas in the study area

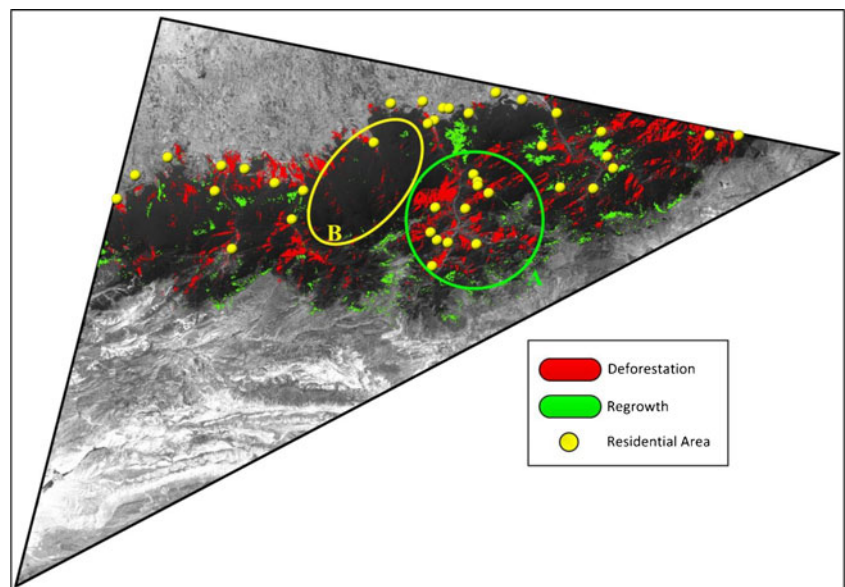
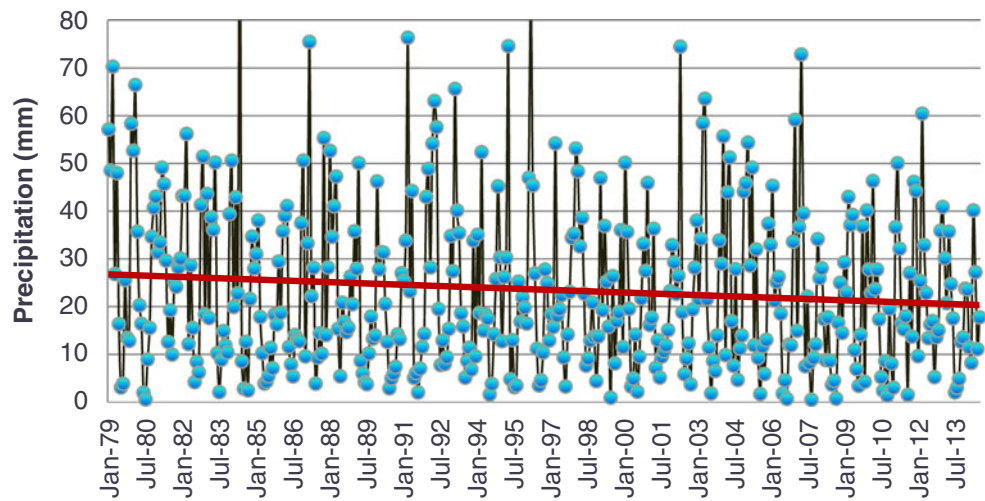




**Fig. 11** Monthly rainfall trend from 1979 to 2013



analysis, severe (high) and medium deforestation conditions presented typically in the northern and eastern parts of the

study regions, respectively. By comparison of the results obtained from SMA with simple vegetation index differences

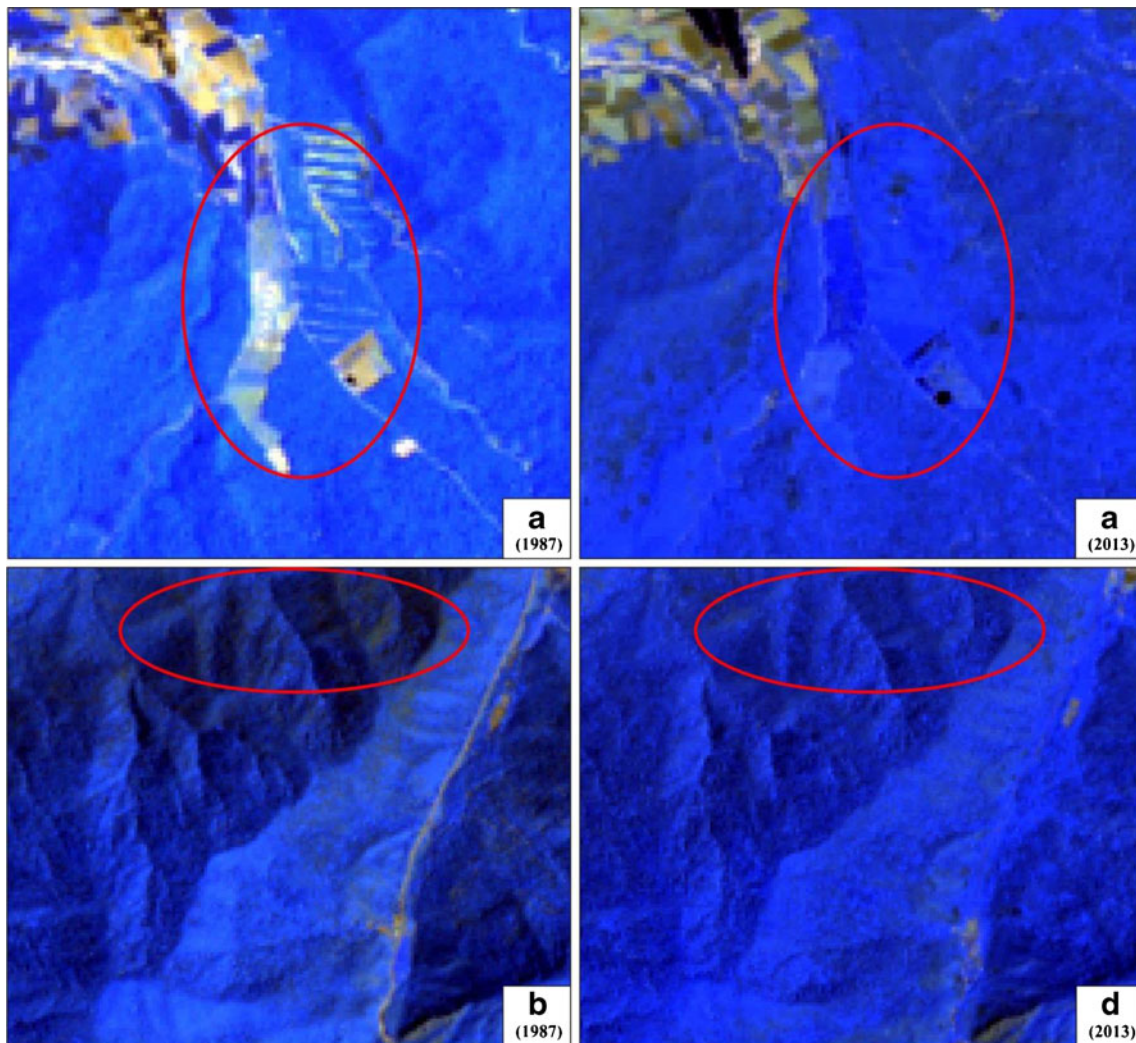


**Fig. 12** Sample of deforestation area that is **a** non-renewable and **b** renewable

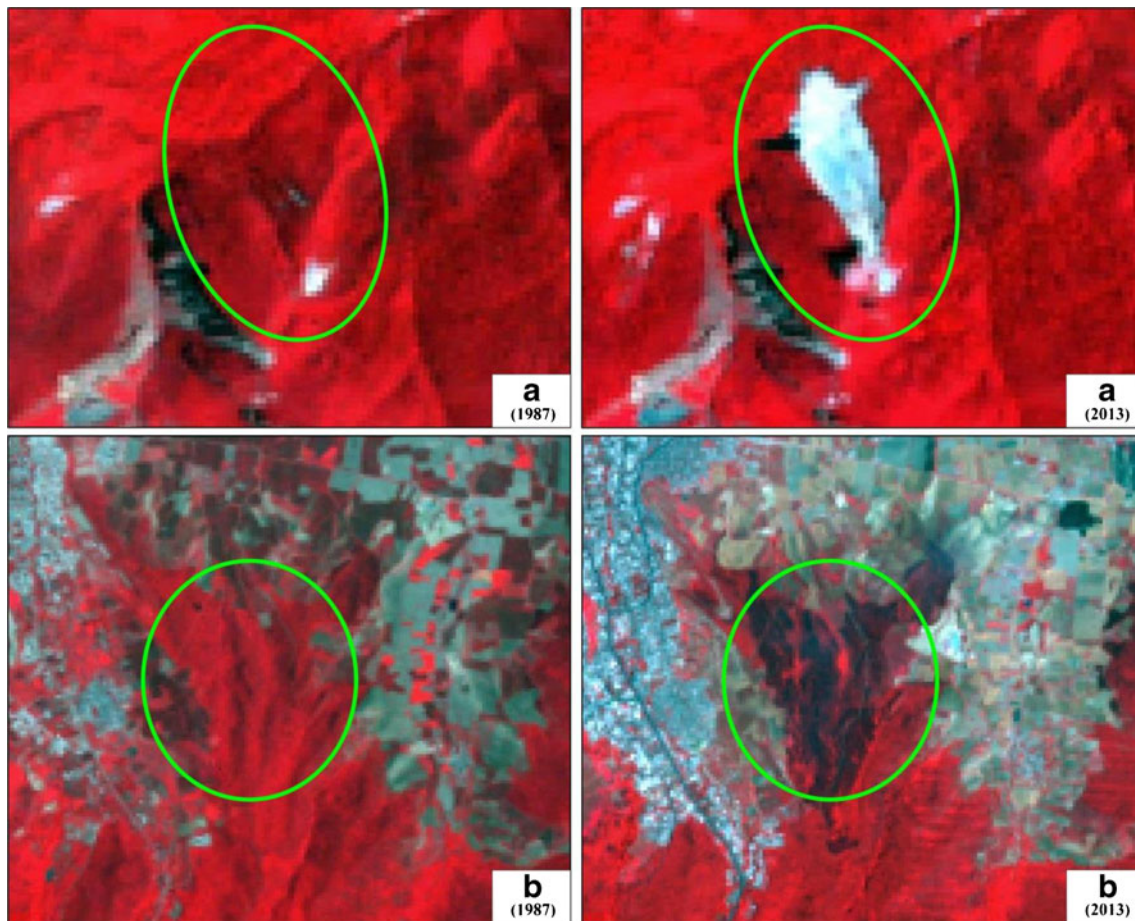


**Fig. 13** Sample of regrowth area that is **a** non-renewable and **b** renewable

(NDVI changes), it was found that although there were no significant differences between the methods used, both some inconsistencies in the results are visible. For example, the area of deforested and regrowth regions in NDVI differences are underestimated about 11 % and overestimated about 17 %, respectively.

Change vector analysis (CVA) demonstrates that deforestation in the Jangal-Abr area has significantly accelerated from 4.6 km<sup>2</sup>/year in the period 1987 and 2000 to 9.6 km<sup>2</sup>/year in period 2010 and 2013 which alarms us with the speed up of this phenomenon in the last few years. It is also observed that there is an apparent link between residential areas and regions exposed to deforestation/regrowth condition. Though in the study area, some forestry projects have been implemented during last decades, e.g., an area of approximately 11,216 ha of the northern hillside was tree planted in 1991, but in contrast, road construction and transforming forests to farming and residential lands have also increased the last two decades and raised the concerns of many local and national NGOs.

**Acknowledgments** This work was completely funded by the Shahrood University of Technology (SUT). Thanks are expressed for review and comments from members of Civil Engineering Department of SUT University and two anonymous reviewers.

## References

- Abbasi A, Mohammadzadeh S (2001) Investigation of world experiences local participation of forest resources management and utilization of successful experience in Iran. In: National proceedings of north forests management and sustainable development conference. Iranian Rangelands and Forests Organization, Tehran
- Achard F, Eva HD, Stibig H-J, Mayaux P, Gallego J, Richards T, Malingreau J-P (2002) Determination of deforestation rates of the world's humid tropical forests *Science* 297:999–1002 doi:10.1126/science.1070656
- Achard F, DeFries R, Herold M, Mollicone D, Pandey D, De Souza JC (2008) Guidance on monitoring of gross changes in forest area, Chapter 3 in GOF-C-GOLD Reducing greenhouse gas emissions from deforestation and degradation in developing countries: a sourcebook of methods and procedures for monitoring, measuring and reporting. GOF-C-GOLD Report version COP13-2. GOF-C-GOLD Project Office. Natural Resources Canada, Alberta, Canada
- Adams JB, Sabol DE, Kapos V, Almeida Filho R, Roberts DA, Smith MO, Gillespie AR (1995) Classification of multispectral images based on fractions of endmembers: application to land-cover change in the Brazilian Amazon. *Remote Sens Environ* 52:137–154
- Amimejad H, Khalilian S, Assareh MH, Ahmadian M (2006) Estimating the existence value of north forests of Iran by using a contingent valuation method *Ecological Economics* 58:665–675 doi:10.1016/j.ecolecon.2005.08.015
- Anderson LO, Shimabukuro YE, Defries RS, Morton D (2005) Assessment of deforestation in near real time over the Brazilian



- Amazon using multi temporal fraction images derived from Terra MODIS. *IEEE Geosci Remote Sens Lett* 3:315–318
- Asner GP, Keller M, Pereira JR, Zweede JC, Silva JNM (2004) Canopy damage and recovery after selective logging in Amazonia: field and satellite studies. *Ecological Applications* 14:280–298. doi:10.1890/01-6019
- Avtar R, Sawada H (2013) Use of DEM data to monitor height changes due to deforestation. *Arab J Geosci* 6:4859–4871. doi:10.1007/s12517-012-0768-2
- Bernstein LS, Adler-Golden SM, Sundberg RL, Ratkowski AJ (2006) Improved reflectance retrieval from hyper- and multispectral imagery without prior scene or sensor information., pp 63622–63628
- Brandt JS, Townsend PA (2006) Land cover conversion, regeneration and degradation in the high elevation Bolivian Andes. *Landsc Ecol* 21: 607–623
- Bryant RG (1996) Validated linear mixture modelling of Landsat TM data for mapping evaporite minerals on a playa surface: methods and applications. *Int J Remote Sens* 17:315–330. doi:10.1080/01431169608949008
- Collado AD, Chuvieco E, Camarasa A (2002) Satellite remote sensing analysis to monitor desertification processes in the crop-rangeland boundary of Argentina *Journal of Arid Environments* 52:121–133 doi:10.1006/jare.2001.0980
- Cracknell AP (1998) Review article Synergy in remote sensing-what's in a pixel? *Int J Remote Sens* 19:2025–2047. doi:10.1080/014311698214848
- Dawelbait M, Morari F (2012) Monitoring desertification in a Savannah region in Sudan using Landsat images and spectral mixture analysis *Journal of Arid Environments* 80:45–55 doi:10.1016/j.jaridenv.2011.12.011
- Downton MW (1995) Measuring tropical deforestation: development of the methods. *Environmental Conservation* 22:229–240. doi:10.1017/S0376892900010638
- Elmore AJ, Mustard JF, Manning SJ, Lobell DB (2000) Quantifying vegetation change in semiarid environments: precision and accuracy of spectral mixture analysis and the normalized difference vegetation index. *Remote Sens Environ* 73:87–102
- Esmacili A, Nasrnia F (2014) Deforestation and the Environmental Kuznets Curve in Iran Small-scale *Forestry* 13:397–406 doi:10.1007/s11842-014-9261-y
- Etteieb S, Louhaichi M, Kalaitzidis C, Gitas I (2013) Mediterranean forest mapping using hyper-spectral satellite imagery. *Arab J Geosci* 6:5017–5032. doi:10.1007/s12517-012-0748-6
- FAO (1990) Forest resources assessment 1990: tropical countries. Paper presented at the FAO Forestry. Rome, Italy
- FAO (2003) State of the world's forests. Italy, Rome
- Fisher P (1997) The pixel: a snare and a delusion. *Int J Remote Sens* 18: 679–685. doi:10.1080/014311697219015
- Gebrehiwot S, Bewket W, Gärdenäs A, Bishop K (2014) Forest cover change over four decades in the Blue Nile Basin Ethiopia: comparison of three watersheds. *Reg Environ Change* 14:253–266. doi:10.1007/s10113-013-0483-x
- Guang-jun W, Mei-chen F, Qiu-ping X, Zeng W Monitoring grassland desertification around the built-up area of the city based on multi-temporal remotely sensed images. In: *Management and Service Science, 2009. MASS'09. International Conference on*, 20–22 Sept. 2009. pp 1–4. doi:10.1109/ICMSS.2009.5303133
- Hashemi S, Fallah Chai M (2013) Investigation of NDVI in relation to the growth phases of beech leaves in forest. *Arab J Geosci* 6:3341–3347
- Hashemi S, Fallah Chai M, Bayat S (2013) An analysis of vegetation indices in relation to tree species diversity using by satellite data in the northern forests of Iran. *Arab J Geosci* 6:3363–3369. doi:10.1007/s12517-012-0576-8
- Jacobson CR (2014) The effects of endmember selection on modelling impervious surfaces using spectral mixture analysis: a case study in Sydney Australia. *Int J Remote Sens* 35:715–737. doi:10.1080/01431161.2013.871594
- Kang S, Choi W (2014) Forest cover changes in North Korea since the 1980s. *Reg Environ Change* 14:347–354. doi:10.1007/s10113-013-0497-4
- Kavian A, Azmoodeh A, Solaimani K (2014) Deforestation effects on soil properties, runoff and erosion in northern Iran *Arab J Geosci* 7: 1941–1950 doi:10.1007/s12517-013-0853-1
- Kelarestaghi A, Jafarian Jeloudar Z (2011) Land use/cover change and driving force analyses in parts of northern Iran using RS and GIS techniques. *Arab J Geosci* 4:401–411. doi:10.1007/s12517-009-0078-5
- Khiry MA, Csaplovics E (2007). Appropriate methods for monitoring and mapping land cover changes in semi-arid areas in North Kordofan (Sudan) by using satellite imagery and spectral mixture analysis. In: *Analysis of Multi-temporal Remote Sensing Images, 2007. MultiTemp 2007. International Workshop on the*, 18–20. pp 1–4. doi:10.1109/MULTITEMP.2007.4293065
- Lunetta RS (1999) Applications, project formulation, and analytical approach. In: Lunetta RS, Elvidge CD (eds) *Remote sensing change detection: environmental monitoring methods and applications*. Taylor & Francis Press, London, pp 1–19
- Mas J-F (2005) Assessing protected area effectiveness using surrounding (buffer) areas environmentally similar to the target area. *Environ Monit Assess* 105:69–80. doi:10.1007/s10661-005-3156-5
- Moridnejad A, Karimi N, Ariya PA (2015) Newly desertified regions in Iraq and its surrounding areas: significant novel sources of global dust particles *Journal of Arid Environments* 116:1–10 doi:10.1016/j.jaridenv.2015.01.008
- Munyati C (2000) Wetland change detection on the Kafue Flats Zambia, by classification of a multitemporal remote sensing image dataset. *Int J Remote Sens* 21:1787–1806. doi:10.1080/014311600209742
- Munyati C, Kabanda T (2009) Using multitemporal Landsat TM imagery to establish land use pressure induced trends in forest and woodland cover in sections of the Soutpansberg Mountains of Venda region Limpopo Province, South Africa. *Reg Environ Change* 9:41–56. doi:10.1007/s10113-008-0066-4
- Phua M-H, Tsuyuki S, Furuya N, Lee JS (2008) Detecting deforestation with a spectral change detection approach using multitemporal Landsat data: a case study of Kinabalu Park, Sabah, Malaysia *Journal of Environmental Management* 88:784–795 doi:10.1016/j.jenvman.2007.04.011
- Rosenberg N (1992) A Commentary on: Deforestation, climate change and sustainable nutrition security: a case study of India. In: Myers N (ed) *Tropical Forests and Climate*. Springer Netherlands, pp 211–213. doi:10.1007/978-94-017-3608-4\_21
- Shimabukuro YE, Smith A (1991) The least-squares mixing models to generate fraction images derived from remote sensing multispectral data *Geoscience and Remote Sensing. IEEE Trans* 29:16–20
- Small C (2001) Estimation of urban vegetation abundance by spectral mixture analysis. *Int J Remote Sens* 22:1305–1334. doi:10.1080/01431160151144369
- Small C (2004) The Landsat ETM+ spectral mixing space *Remote Sensing of Environment* 93:1–17 doi:10.1016/j.rse.2004.06.007
- Smith MO, Johnson PE, Adams JB (1985) Quantitative determination of mineral types and abundances from reflectance spectra using principal components analysis. *Journal of Geophysical Research Solid Earth* 90:C797–C804. doi:10.1029/JB090iS02p0C797
- Somers B, Verbesselt J, Ampe EM, Sims N, Verstraeten WW, Coppin P (2010) Spectral mixture analysis to monitor defoliation in mixed-aged *Eucalyptus globulus* Labill plantations in southern Australia using Landsat 5-TM and EO-1 Hyperion data *International Journal of Applied Earth Observation and Geoinformation* 12:270–277 doi:10.1016/j.jag.2010.03.005

- Somers B, Asner GP, Tits L, Coppin P (2011) Endmember variability in spectral mixture analysis: a review *Remote Sensing of Environment* 115:1603–1616 doi:[10.1016/j.rse.2011.03.003](https://doi.org/10.1016/j.rse.2011.03.003)
- Tucker CJ (1979) Red and photographic infrared linear combinations for monitoring vegetation *Remote Sensing of Environment* 8:127–150 doi:[10.1016/0034-4257\(79\)90013-0](https://doi.org/10.1016/0034-4257(79)90013-0)
- Tucker CJ, Townshend JRG (2000) Strategies for monitoring tropical deforestation using satellite data. *Int J Remote Sens* 21:1461–1471. doi:[10.1080/014311600210263](https://doi.org/10.1080/014311600210263)
- Veraverbeke S, Somers B, Gitas I, Katagis T, Polychronaki A, Goossens R (2012) Spectral mixture analysis to assess post-fire vegetation regeneration using Landsat Thematic Mapper imagery: accounting for soil brightness variation *International Journal of Applied Earth Observation and Geoinformation* 14:1–11 doi:[10.1016/j.jag.2011.08.004](https://doi.org/10.1016/j.jag.2011.08.004)
- Vitousek PM (1994) Beyond global warming: ecology and global change *Ecology* 75:1862–1876 doi:[10.2307/1941591](https://doi.org/10.2307/1941591)
- Wertz-Kanounnikoff S (2008) Monitoring forest emissions: a review of methods. Center for International Forestry Research (CIFOR). Bogor, Indonesia
- Wessman CA, Bateson CA, Benning TL (1997) Detecting fire and grazing patterns in tallgrass prairie using spectral mixture analysis. *Ecol Appl* 7:493–511. doi:[10.1890/1051-0761\(1997\)007\[0493:DFAGPI\]2.0.CO;2](https://doi.org/10.1890/1051-0761(1997)007[0493:DFAGPI]2.0.CO;2)